Eur. Phys. J. B **9**, 137–147 (1999)

THE EUROPEAN PHYSICAL JOURNAL B

EDP Sciences

Polymer-mediated interactions of fluid membranes in a lyotropic lamellar phase: a small angle X-ray and neutron scattering study

G. Bouglet and C. Ligoure[a]

Groupe de Dynamique des Phases Condensées[b], C.C. 26, Université Montpellier II 34095 Montpellier Cedex 5, France

Received 20 January 1998

Abstract. Small angle X-ray and neutron scattering data on an effective three-component lamellar phase composed of water, a non adsorbing water-soluble polymer (polyvynilpyrolidone), fluid membranes, made from a mixture of a cationic surfactant (cetylpiridiumchloride) and a cosurfactant (hexanol), are presented for various membrane as well as polymer concentrations. The data are fitted with a recently proposed model which takes into account the geometry and the fluctuations of these periodic structures. This allows a quantitative study of the polymer contribution to the smectic compression modulus $\bar{B}$ of the lamellar phase. Four different regimes of polymer confinement are expected. The associated variations in $\bar{B}$ are compared to a recent theoretical model, which predicts the polymer-mediated contribution to the smectic compression modulus.

PACS. 61.30.Eb Experimental determinations of smectic, nematic, cholesteric, and other structures – 82.70.-y Disperse systems – 61.25.Hq Macromolecular and polymer solutions; polymer melts; swelling

1 Introduction

The lamellar phase L_α is perhaps the best characterized lyotropic liquid crystalline phase known to date. Often encountered in phase diagrams of surfactant systems, it consists of infinite planar bilayers of one or more amphiphilic components periodically stacked in space, separated by a solvent. In the past twenty years, much attention has been focused on the understanding of the interactions between those membranes [1]. Among these interactions, the dominant repulsive forces which stabilize an expanded lamellar structure are the electrostatic interaction (for ionic systems) and the undulation or Helfrich's interaction [2]. Nowadays increasing interest is directed towards ternary lamellar systems of surfactant, water and polymer [3–14]. Previous studies have shown that added macromolecules (guest component of the lamellar phase) can occupy a variety of sites in such systems. Indeed, polymer molecules can be confined within the water layers [4–8], fully incorporated in the surfactant bilayers [10], localized both in the bilayers and in the solvent [9], or even adsorb onto the membranes by a specific group [11–14].

The experimental system we have studied belongs to the "doped-solvent lamellar phases" [15] where the guest component (a polymer in our case) does neither incorporate into nor adsorbs onto the surfactant bilayer but remains in the intervening solvent. The underlying L_α phase is the ternary system CPCl (cetylpyridinium chloride)/hexanol/water (for which we have the most extensive set of structural data [16]) in which we incorporate a large water-soluble polymer PVP (polyvinylpirilidone) [4–6]. In pure water (without added salt), the smectic order is stabilized by strong long-range electrostatic interactions (CPCl is a cationic surfactant) and we have experimental evidences, that the polymer is effectively located between the bilayers and does not penetrate them, so that the confinement is effective and the adsorption regime is avoided [6]. Hence this system provides an experimental realization of the idea of a polymer solution confined into infinite slits [17–19].

In a previous paper [5], we have shown that the presence of a non adsorbing polymer in the solvent of the lamellar phase induces an effective destabilizing interaction between the bilayers which depends both on the smectic periodicity d and on the volume fraction of the polymer in the solvent $\bar{\Phi}$ [18]. This interaction is of purely entropic origin, similar to the depletion interaction between colloidal particles in a polymer solution. We have calculated the non adsorbing polymer contribution to the layer compression modulus $\bar{B}$ which is one of the three fundamental smectic elastic constants and is directly related to the bilayer/bilayer interactions. This contribution reflects the four different regimes of polymer confinement within infinite slits, which will be reviewed in Section 3 [17, 18]. In all regimes, this contribution is *negative* meaning that the polymer-mediated interaction tends to destabilize the smectic order. However, in absence of added salt, and for highly charged membranes this destabilizing interaction can never compete with the stabilizing electrostatic

[a] e-mail: ligoure@gdpc.univ-montp2.fr
[b] UMR UMII/CNRS 5581

interaction [5–7]. This fact explains why in our experimental system, we are able to incorporate polyvinylpyrolidone in all proportions, without any modification of the structure of the lamellar phase, which remains stable against phase separation. On the contrary, lamellar/lamellar phase separations can be encountered in these ternary lamellar systems, by decreasing the electrostatic interaction. This can be achieved by adding salt [4,5] and thereby screening the electrostatic interaction, or by diminishing the surface charge density of the bilayers [7]. In both experimental situations our predictions allowed a quantitative interpretation of several critical points of polymer-induced lamellar/lamellar phase separations encountered, in two different surfactant systems [5,7].

The goal of this paper is to measure the layer compression modulus $\bar{B}$ of the polymer-containing lamellar phase in the various regimes of polymer confinement. Doing so, we also investigate the four different regimes of polymer confinement within infinite slits [17].

Small angle X-ray and neutron scattering have been recognized as a powerful technique for the study of the organization as well as the fluctuations of various self-assembling systems. Quantitative treatments of the X-ray (or neutron) scattering patterns of a smectic phase, allow to measure the dimensionless number, η Caillé parameter) [20] characterizing the power-law singularities at the Brag peaks [1,20–27], η is defined in terms of the smectic elastic constant by:

$$\eta = \frac{q_0^2 k_B T}{8\pi\sqrt{K\bar{B}}} \quad (1)$$

where K is the smectic curvature modulus (related to the bilayer bending modulus and to the smectic periodicity d according to $K = \kappa/d$) and q_0 is the position of the first Brag singularity: $q_0 = 2\pi/d$.

In a recent paper [6], we have investigated the effect of the incorporation of PVP on the bending modulus κ of the CPCL/hexanol/water lamellar phases by deuterium solid-state NMR technics. It was found that κ is insensitive to the amount of polymer in the lamellar phase in agreement with the theoretical predictions of Brooks [28]. These treat the contribution of a *non adsorbing* polymer to the bending modulus of a surfactant bilayer. The measured value of κ with the NMR technics is $\kappa = 1.7 \pm 0.5\, k_B T$. Consequently $\bar{B}$, which contains the thermodynamics of polymer confinement, is directly deduced from the measurement of η. The experimental powder spectra have been fitted with an analytical model recently proposed by Nallet *et al.* [23]. It allowed us to fit the powder spectra of the lyotropic lamellar phases not only in the vicinity of the Bragg-peak position, but throughout the entire q range (except of for very low q). This fitting process has been successfully used for another system [29].

The outline of the paper is as follows: In Section 2, we present the polymer-surfactant system, we have studied and we describe the fitting process of the small angle X-ray or neutron scattering data performed on the lamellar phase. In Section 3, we review the different dominant contributions to the layer compression modulus $\bar{B}$ and check experimentally their additivity. Finally in Section 4, we report on the variations of the total layer compression modulus extracted from the scattering patterns and discuss these results in terms of the four regimes of polymer confinement within infinite slits.

2 Experimental

2.1 Sample preparation

The experimental system was presented elsewhere [4–6]: we incorporate a large water-soluble polymer into a L_α phase made of charge bilayers. The L_α phase was obtained using the ternary system CPCl/hexanol/water at room temperature. In all samples the alcohol to surfactant weight ratio is fixed: $m_{hex}/m_{CPCL} = 0.9$, which corresponds to the alcohol rich domain of the lamellar phase with an oily streak structure [29]. The bending modulus of the CPCL/hexanol bilayer is $\kappa = 1.7 \pm 0.5\, k_B T$ and is not changed by the addition of any amount of polymer. Polyvinylpyrolidone (PVP), which has a monomer length $a = 3$ Å in water [30], was used as added polymer fraction. Water and brine up to 0.5 M NaCl concentration are good solvents for PVP [31]. The reported number average molecular weight is $M_n = 360\,000$ g/mol; and the measured polydispersity index is about 2. The radius of gyration as determined by light scattering, is about 60 nm in water and the overlapping weight concentration Φ^* is found close to 0.15% [4].We have also used for some series of samples PVP of much smaller molecular weight $M_n = 10{,}000$ g/mole. The experimental protocol to obtain homogeneous non oriented samples is the following: surfactant, alcohol and water (heavy water for neutron experiments) are mixed, in order to obtain the lamellar phase; the polymer is then incorporated and dissolved along several cycles of heating and centrifugation. The samples are then left to equilibrate at 20 °C for several weeks. Direct observation of the samples between crossed polarizers shows in all cases homogeneous birefringence; moreover we have observed that addition of polymer induces the proliferation of spherulite-like defects in the lamellar phase, implying a powder orientation in all samples. The samples are then sealed in capillaries (diameter 1 mm) for X-ray experiments or flat cells (1 or 2 mm) for neutron experiments.

2.2 X-ray instrument

Small angle X-rays experiments were performed at the beam line BL4/Id2 of the European Synchrotron Radiation Facility in Grenoble [32]. The wavelength of the X-rays was 1 Å ($D_1/l = 3 \times 10^{-4}$), the incident beam is collimated with a set of slits and guard slits that defined an irradiated area on the sample of 0.5×1 mm^2. The detector is a 2D-gas filled detector (180 mm in diameter) coupled with a delay-line electronics. The distance between sample and detector was varied between 0.8 and 10 m. For our experiments, the q range lied between 0.05 and 0.4 Å^{-1}.

The scattering vector is defined as $q = (4\pi/\lambda)\sin(\theta)$ with 2θ being the scattering angle. The total resolution $\Delta q/q$ of detection is mainly defined by the detector and was 4×10^{-2} at 3×10^{-2} Å^{-1}. The 2D-data were corrected with respect to the response of the detector and normalized by the incident flux. Then an azimuthal averaging was applied in order to obtain 1D data for the intensity distribution $I(q)$. The background subtraction and the transmission correction have been adjusted at the end because of an incertitude in the thickness of the capillaries.

2.3 Neutron instrument

Neutron experiment were performed at the beam line D22 of the Laue Langevin Institute in Grenoble. The wavelength of the neutron was 8 Å with a resolution $\Delta\lambda/\lambda$ of about 10%. The size of the 2D-detector is 1 m^2 divided in 128×128 0.75 cm^2 cells. Two distances between detector and sample were used (1.5 and 8 m), hence covering a q-range of 0.05−0.4 Å^{-1}. We first set the detector to the 1.5 m distance covering the "large angle" scattering, and then to 8 m covering the "small angle" scattering. The spectra were corrected for the background, incoherent scattering and detector defaults.

2.4 Scattering intensity of the powder spectra

Various models for calculating the scattering intensity of the lyotropic lamellar phase have been suggested in the past years [20–27]. The scattering intensity of periodic systems can be calculated in term of a form and a structure factor. We chose the recent analytical model of Nallet *et al.* [23] because of its simplicity and the rapidity of the fitting calculations. Despite its simplicity, it appears that the obtained η values are strictly identical to those obtained from fitting the same data with a more sophisticated model which requires much heavier numerical calculations [33], provided that the smectic order is sufficiently strong. Performing the powder averaging in the limit $q \gg \Delta q$, the experimentally recorded intensity scattered by an irradiated volume V reads [23]:

$$I(q) = \frac{2\pi V P(q) S(q)}{dq^2} \qquad (2)$$

where $S(q)$ is resolution-limited structure factor given by equation (9) of reference [23] (it is a function of η and d), and $P(q)$ is the form factor which depends on the nature of the radiation as discussed below (note: also the apparatus function is taking into account). With this proposed model, the number of free parameters is only four (respectively three) for the X-ray (respectively neutron) experiments: the scaling factor, A_0, two structure factor parameters (the periodicity d and the dimensionless parameter η) and one (respectively zero) form factor parameter.

The number of lamellae (N in Eq. (9) of Ref. [23]) was chosen to be 90 in order to satisfy the condition $N\Delta q/q_0 \gg 1$, where $q_0 = 2\pi/d$ is the position of the first order Brag peak. By varying N from 50 to 150 we ascertain that the corresponding variation of η is less than 0.01. The corresponding uncertainty is then $\Delta\eta = 0.01$.

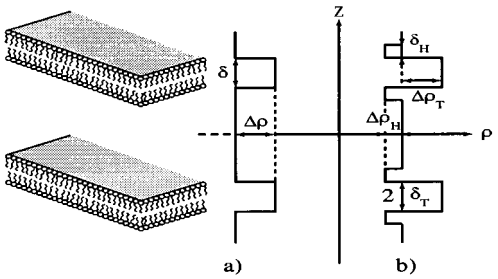

Fig. 1. Schematic scattering length density profiles, ρ, along the normal of the bilayer: a) neutron scattering experiment, b) X-ray scattering experiment.

The experimental resolution depends on the nature of the radiation and is modeled by a Gaussian profile of width, Δq, for the apparatus function

$$\Delta q_{\mathrm{X-ray}} = 0.0016 \text{ Å}^{-1}$$
$$\Delta q_{\mathrm{neutron}} = 0.0025 \text{ Å}^{-1}.$$

The smectic period d is directly measured from the first order Brag-peak position ($d = 2\pi/q_0$); it is well defined apart from a negligible uncertainty.

2.4.1 Neutron and X-ray form factor

For X-ray scattering experiments, the profile $\rho(z)$, arises from the electron density distribution across the bilayer. We employ the reasonable two-square profile as used in [23], where δ_{H} and δ_{T} are respectively the lengths of the hydrated polar head and hydrophobic tail as sketched in Figure 1. The scattering thickness of the bilayer is $\delta = 2(\delta_{\mathrm{H}} + \delta_{\mathrm{T}})$. We measured classically δ from a dilution line [10,17] $\delta = 26 \pm 0.05$ Å. $\Delta\rho_{\mathrm{H}}$, $\Delta\rho_{\mathrm{T}}$ are the difference between the electronic density of the solvent, ρ_{S}, and of the aliphatic part ($\Delta\rho_{\mathrm{H}} = \rho_{\mathrm{H}} - \rho_{\mathrm{S}}$) and of the hydrophobic part ($\Delta\rho_{\mathrm{T}} = \rho_{\mathrm{T}} - \rho_{\mathrm{S}}$) of the surfactant bilayer respectively. Addition of polymer leads to a weak change in the electronic density of the solvent ($\rho_{\mathrm{H_2O}} = 0.33$ e/Å^3, $\rho_{\mathrm{PVP}} = 0.35$ e/Å^3). The X-ray form factor is then:

$$P(q)_{\mathrm{X-ray}} = \frac{4\Delta\rho_{\mathrm{H}}^2}{q^2}\Big\{ \sin(q(\delta_{\mathrm{H}} + \delta_{\mathrm{T}})) - \sin(q\delta_{\mathrm{T}}) + \frac{\Delta\rho_{\mathrm{T}}}{\Delta\rho_{\mathrm{H}}}\sin(q\delta_{\mathrm{T}})\Big\}^2. \qquad (3)$$

The variation of the polymer concentration in the solvent causes ρ_{S} to vary only little. However, to take this variation into account, the $\Delta\rho_{\mathrm{T}}/\Delta\rho_{\mathrm{H}}$ term in equation (3) is set to be a fitting parameter; the $\Delta\rho_{\mathrm{H}}^2$ term in equation (3) is included in the scaling factor A_0 of equation (2): $A_0 = \dfrac{8\pi}{d}\Delta\rho_{\mathrm{H}}^2$, and therefore, this scaling factor depends on the polymer concentration too. There are only two unknown parameters in the X-ray form factor δ_{H} and

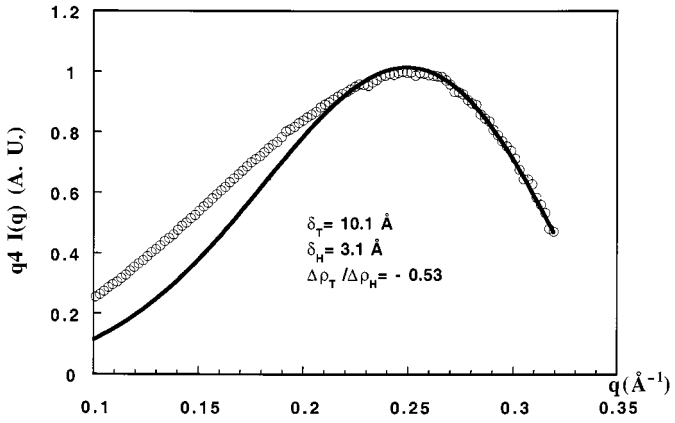

Fig. 2. Selected dilute sample ($\Phi_S = 13.3\%$) of q^4 times the X-ray intensity profile with fit to equation (3) at large angles. Fitting parameters of the form factor are: $\delta_H = 3.1$ Å, $\delta_T = 10.1$ Å and $\Delta\rho_T/\Delta\rho_H = -0.53$.

$\Delta\rho_T/\Delta\rho_H$. We first determine these two parameters, by fitting the theoretical expression (3) for the large wave vector part ($q > 0.1$ Å^{-1}) of the intensity scattered by a dilute sample ($\Phi_S = 13.3\%$), without polymer. For this we assume that for this large q, range the structure factor has reached its asymptotic value ($S(q \gg q_0) = 1$). These parameters are obtained by fitting to the data with q^4 times the predicted intensity (see Fig. 2): $\delta_H = 3.1$ Å, $\delta_T = 10.1$ Å and $\Delta\rho_T/\Delta\rho_H = -0.53$. In the following, the two values δ_H and δ_T are fixed, whereas the ratio $\Delta\rho_T/\Delta\rho_H$ is a free parameter which takes into account the polymer effect on the variation of the electronic density of the solvent.

For neutron diffraction patterns the square-Gaussian profile is a reasonable model for describing the length density profile, $\rho(z)$, of bilayers [23].

$$P(q)_{\text{neutron}} = \frac{2\Delta\rho^2}{q^2}\left[1 - \cos(q\delta)\exp\left(-\frac{q^2\sigma^2}{2}\right)\right] \quad (4)$$

here σ is arbitrarily fixed at $\delta/4$ and $\Delta\rho$ is the length density contrast between the hydrophobic part of the surfactant molecule and the solvent. In this model, the density of the hydrophilic part (head group) of the surfactant is assumed to be the same as that of the solvent, so that the effective thickness of the lamellar membrane is $\delta_{\text{eff}} = \delta - 2\delta_H$ about 20 Å. The scattering lengths densities of each compound are the following:
$\rho_{D_2O} = 6.39 \times 10^{10}$ cm^{-2}, $\rho_{PVP} = 1.254 \times 10^{10}$ cm^{-2}, $\rho_{CPCL} = 0.276 \times 10^{10}$ cm^{-2}, $\rho_{hex} = -0.322 \times 10^{10}$ cm^{-2}. From these data, it is clear PVP cannot be matched by a given D_2O/H_2O mixture ($\rho_{H_2O} = -0.56 \times 10^{10}$ cm^{-2}), without leading to a very poor membrane/solvent contrast. Contrary to X-ray experiments, there are only three fitting parameters in neutron experiments: the scaling factor A_0 of equation (2): $A_0 = \frac{4\pi}{d}\Delta\rho^2$ remains a free fitting parameter since it includes the polymer effect on the contrast ($\Delta\rho^2$ parameter) [34].

2.4.2 Fitting process

Whatever the nature of the radiation, the fits were performed with the following free parameters: the scaling factor A_0, the smectic periodicity, d, the Caillé parameter η and for X-ray experiments only, the ratio of length density profile, $\Delta\rho_T/\Delta\rho_H$. The fitting q-range was chosen between $q_0/1.5 \leq q \leq 2.5\ q_0$. The upper limit of q allows to fit simultaneously the first and the second harmonics of all lamellar phases, and the lower limit avoids the small angle excess scattering, which is not properly described by the Nallet model. The numerical fitting process is very sensitive to the starting values of the fitting parameters, because there are several local minima in the space of the fitting parameters. In order to control the effects of the starting condition on their own final values and particularly on the η parameter, we performed the fits with a large number of sets of free parameters. For a starting value of η lying over the all definition range ($0 < \eta < 1$), the variations of the final values of η are less than 0.005, without any significant modification of the fits; the smectic periodicity, d, remains always unchanged, whatever the starting smectic periodicity is. On the contrary, we have a correlation between the best fitting values of the scaling factor A_0 and the contrast parameter $\Delta\rho_T/\Delta\rho_H$ in X-ray spectra: the best fitting profiles are obtained for both A_0 and $\Delta\rho_T/\Delta\rho_H$ on the order of unity. The corresponding uncertainty on the final fitting value of η is about 0.02.

With the above careful analysis of the fitting process, we conclude that the uncertainty of the measurement of the Caillé parameter, η is $\Delta\eta = \pm\ 0.02$.

The experimental layer compression modulus is then obtained by inserting the measured value of η into equation (1), one obtains:

$$\bar{B}_{\text{exp}} = \frac{q_0^3(k_BT)^2}{32\pi k_c\eta^2} \quad (5)$$

with $k_c = \dfrac{\kappa}{k_BT} \simeq 1.7$ [6].

As shown in reference [6], the value of the elastic bending modulus κ is the same whatever is the polymer concentration. Consequently, the uncertainty in the measurement of the experimental layer compression modulus is

$$\frac{\Delta\bar{B}_{\text{exp}}}{\bar{B}_{\text{exp}}} = \frac{2\Delta\eta}{\eta}\,. \quad (6)$$

3 Smectic compression modulus of a non-adsorbing polymer containing lamellar phase

3.1 Theoretical background

In a recent publication [5], we reported on a simple theoretical model predicting the smectic compression modulus of any solvent-doped lamellar phase. This model requires only the knowledge of the free energy, V, per unit bilayer area. It was applied to the case of an electrostatically stabilized lamellar phase doped with non-adsorbing

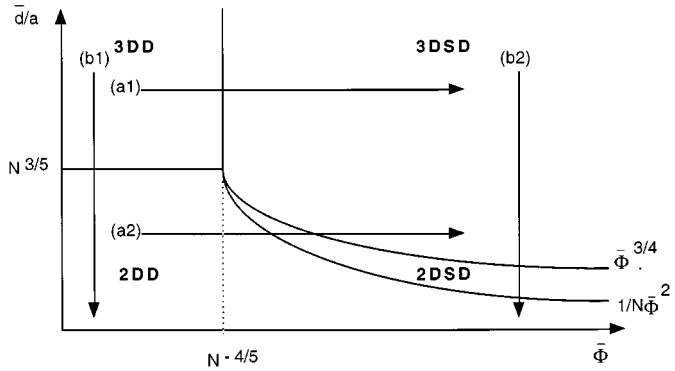

Fig. 3. Diagram of the four different confinement regimes for a solution of a water soluble non-adsorbing polymer in a lamellar phase (from Ref. [15]). X-axis: volume fraction of polymer in the solvent. Y-axis: solvent layer thickness between two adjacent bilayers normalized to the monomer length of the polymer.

polymers, and allowed successfully the quantitative analysis of several critical points of lamellar/lamellar phases separations encountered in these systems [5,7]. We also showed that in the present experimental system there are three dominant contributions to the intermembrane interaction V: two repulsive ones, the electrostatic interaction $V_{\rm elec}(\bar{d})$ and the Helfrich's interaction $V_{\rm Helf}(\bar{d})$ and one destabilizing interaction: the polymer-mediated interaction, $V_{\rm pol}(\bar{d},\bar{\Phi})$; $\bar{d} = d - \delta$ denotes the interlayer solvent thickness and $\bar{\Phi}$ is the volume fraction of polymer in the solvent. Other interactions, like the hydratation, or van der Waals interactions can be safely neglected in our system (for the dilution range of our samples, their contributions to the layer compression modulus are two order of magnitude smaller than the electrostatic contribution [5]). Note that the Helfrich's repulsion is in general much smaller than the electrostatic repulsion except for concentrated samples in brine.

The polymer-mediated interaction $V_{\rm pol}$ has been analyzed in reference [6], by extending previous works [17,18]. Four different regimes of polymer confinement within the lamellae exist, depending on $\bar{\Phi}$ and $\bar{d}$, with smooth crossovers between them as shown in Figure 3. $R_{\rm F} = aN^{3/5}$ is the Flory radius of a polymer chain (N is the polymerization index and a denotes the Kuhn statistical length) and Φ^* is the overlap volume fraction ($\Phi^* = Na^3/R_F^3$).

i) For $\bar{d} > R_{\rm F}$ and $\bar{\Phi} < \Phi^*$ the solvent is a three-dimensional dilute solution of polymer chains (3DD regime). The chains do not overlap and retain their average spherical coil conformation.

ii) For $\bar{d} > a\Phi^{-3/4}$ and $\bar{\Phi} > \Phi^*$ the solvent is a three dimensional semi-dilute solution of polymer chains (3DSD regime). The chains overlap but still remain non squeezed.

iii) For $a/(N\bar{\Phi}^2) < \bar{d} < a\bar{\Phi}^{-3/4}$ and $\bar{\Phi} > \Phi^*$: the chains both overlap and are squeezed by the slits. This regime is called two dimensional semi dilute regime (2DSD regime).

iv) For $\bar{d} < R_{\rm F}$ and $\bar{\Phi} < \Phi^*$, or $\bar{d} < a/(N\bar{\Phi}^2)$ and $\bar{\Phi} > \Phi^*$: the solvent is a two-dimensional dilute solution of polymer chains (2DD regime). The chains do not overlap but are squeezed.

From the definition of the layer compression modulus of a doped solvent lamellar phase one obtains the following predictions for $\bar{B}_\mu^{\rm pol}$ the polymer contribution to $\bar{B}$:

D3D regime

$$\bar{B}_\mu^{\rm pol} = -\frac{4k_{\rm B}TR_{\rm F}^2 d\bar{\Phi}}{a^3 N\bar{d}^3}\left[1+\log\left(\bar{\Phi}/\left(1-2\frac{R_{\rm F}}{\bar{d}}\right)\right)\right]^2 \cong -4\frac{k_{\rm B}TN^{1/5}d\bar{\Phi}}{a\bar{d}^3} \quad (7a)$$

D2D regime

$$\bar{B}_\mu^{\rm pol} = d\frac{5\alpha k_{\rm B}T}{9\bar{d}^4}\left(\frac{a}{d}\right)^{1/3}\bar{\Phi}\left(-5\alpha N + 8\left(\frac{\bar{d}}{a}\right)^{5/3}\right) \cong -\frac{25\alpha^2 k_{\rm B}T}{9}N\bar{\Phi}\left(\frac{a}{d}\right)^{1/3}\frac{d}{\bar{d}^4} \quad (7b)$$

3DSD regime

$$\bar{B}_\mu^{\rm pol} = -d\frac{k_{\rm B}T}{a\bar{d}^3}\frac{9\rho^2\bar{\Phi}}{\frac{45}{16}\beta\bar{\Phi}^{1/4}+\frac{3}{2}\rho\frac{a}{d}\bar{\Phi}^{1/2}} \cong -\frac{16\rho^2 k_{\rm B}T}{5\beta a}\frac{d}{\bar{d}^3}\bar{\Phi}^{3/4} \quad (7c)$$

2DSD regime

$$\bar{B}_\mu^{\rm pol} = d\left[\frac{25}{9}\frac{\delta k_{\rm B}T}{a^4}\left(\frac{a}{\bar{d}}\right)^{8/3}\bar{\Phi} + \frac{\eta k_{\rm B}T\bar{\Phi}^3}{2a^4} - \frac{25k_{\rm B}T\delta^2}{54a^4\eta}\left(\frac{a}{\bar{d}}\right)^{16/3}\bar{\Phi}^{-1}\right] \cong -\frac{25\delta^2 k_{\rm B}Td}{54a^4}\left(\frac{a}{\bar{d}}\right)^{16/3}\bar{\Phi}^{-1} \quad (7d)$$

where α is an unknown numerical prefactor of the order of unity, β and ρ are universal prefactors calculated in reference [18]. ($\beta \cong 1.97$ and $\delta \cong 0.985$). For δ and η Brooks and Cates have proposed approximate values $\delta \cong 2.22$ and $\rho \cong 1.72$.

In summary, we have obtained simple analytical expressions for the non adsorbing polymer contribution to the smectic compression modulus of a polymer-containing

lamellar phases. In the four expected regimes, this contribution is *negative*, meaning that the effective intermembrane interaction mediated by the trapped polymers is *attractive*. It should be noted, that $\bar{B}_\mu^{\rm pol}$ is *a non monotonic function of the polymer concentration*, at constant membrane concentration. For instance, $\bar{B}_\mu^{\rm pol} \propto -\bar{\Phi}^{-1}$ (respectively $-\bar{\Phi}^{3/4}$) in the 2D-S-D (respectively 3D-S-D) regime. Finally, the expressions we have obtained are valid *only far away* from the boundaries between the different polymer confinement regimes, as explained in details in reference [5]. In particularly there are spurious discontinuities in $\bar{B}_\mu^{\rm pol}$ at the crossovers between the different regimes.

Two case have to be considered for the electrostatic contribution $\bar{B}^{\rm elec}$ to the smectic compression modulus [7]:

$$\bar{B}^{\rm elec} = \frac{\pi k_{\rm B}T}{2l_{\rm B}}\frac{d}{\bar{d}^3}(1-3\tau+6\tau^2+\dots) \qquad \text{if [NaCl]} = 0 \tag{8a}$$

where $\tau = \Sigma/(\bar{d}l_{\rm B})$, $l_{\rm B} = e^2/(4\pi\varepsilon kT) \approx 7.2$ is the Bjeerum length in water at room temperature and Σ is the surface area per charged head of the membrane. In our system, $\Sigma = 98$ Å^2, since the composition of the membrane is fixed in all samples.

In the case of screened interactions (added salt):

$$\bar{B}^{\rm elec} = \frac{4k_{\rm B}Td}{\pi\lambda_{\rm D}'^3 l_{\rm B}}\gamma^2 {\rm e}^{-\bar{d}/\lambda_{\rm D}'} \qquad \text{if [NaCl]} \neq 0 \tag{8b}$$

where $\gamma = \tanh\left[\frac{1}{2}{\rm arcsinh}\left(2\pi\frac{l_{\rm B}\lambda_{\rm D}'}{\Sigma}\right)\right]$ and $\lambda_{\rm D}'(\text{Å}) = \frac{3.04}{\sqrt{c_{\rm s}'}}$ is the relevant Debye length. Note that $c_{\rm s}'$ (mol/l) is the effective salinity of the solution [35], and is related to the mean salinity [NaCl] *via* the equation: [NaCl] $\cong c_{\rm s}'\left(1-4\frac{\lambda_{\rm D}'}{\bar{d}}\right)$.

The contribution of Helfrich's interactions to $\bar{B}$ reads:

$$\bar{B}^{\rm und} = \frac{9\pi^2(k_{\rm B}T)^2 d}{64\kappa\bar{d}^4}\,. \tag{9}$$

3.2 Additivity of the dominant interactions

If we assume that the electrostatic, Helfrich and polymer-mediated interactions are not coupled, the total intermembrane interaction, V, can be simply written as the sum of the electrostatic, Helfrich and polymer-mediated interactions, *i.e.*: $V = V_{\rm elec} + V_{\rm und} + V_{\rm pol}$. As a consequence, the total smectic compression modulus is also the sum of the polymer-mediated and repulsive contributions:

$$\bar{B} = \bar{B}_\mu^{\rm pol} + \bar{B}^{\rm elec} + \bar{B}^{\rm und}. \tag{10}$$

Such an assumption is valid as long as $\bar{\Phi} < 0.1$. Indeed, for higher polymer concentration, the variation of the dielectric permittivity of the PVP solution (measured in Ref. [36]) cannot be neglected and will decrease the electrostatic interaction between the membranes. However, for all series of samples we have studied, this effect is negligible.

In order to check experimentally the validity of the additivity hypothesis, we have investigated two series of salted lamellar samples, increasing the polymer concentration from 0 to 8.5%. The salinity is fixed at [NaCl] = 0.06 mol/l for the first series and [NaCl] = 0.09 mol/l for the second series. The membrane volume fractions are identical for the two series and correspond to a thickness of solvent inbetween two adjacent bilayers ($\bar{d} = 50$ Å). In Figures 4a and 4b, we show for each series, one example of the X-ray profiles with the corresponding fits. In Figure 5 we have plotted the measured smectic compression modulus (obtained as described in the preceding section) *versus* the polymer volume fraction in the solvent for the two salinities. The most interesting feature is that the variation $\bar{B}$ of as a function $\bar{\Phi}$ for the two salinities can be superposed by a vertical translation of length $\Delta\bar{B} \approx 0.7$ Atm. Moreover this shift corresponds roughly to the difference between the electrostatic contributions to the smectic compression modulus at the two different salinities [NaCl] = 0.06 mol/l and [NaCl] = 0.09 mol/l. Indeed, these contributions can be calculated from equation (8b). One obtains:

$$\begin{aligned}\Delta\bar{B}_{\rm theo} &= \bar{B}^{\rm elec}(0.06\text{ mol/l}) - \bar{B}^{\rm elec}(0.09\text{ mol/l})\\ &\simeq 0.6\text{ Atm.}\end{aligned}$$

This result shows the validity of the additivity hypothesis of the dominant interactions.

4 Variation of the smectic compression modulus in the different regimes of polymer confinement

In order to investigate all polymer-confinement regimes, we have studied four series of samples. Each series corresponds to a particular path in the diagram of polymer-confinement regimes (see Fig. 2). Two horizontal paths (series a1 and a2 in Fig. 3) allow a systematic study of the variation of $\bar{B}$ as function of $\bar{\Phi}$ through out the various regimes of polymer confinement: path a1 intersects the 3DD and 3DSD regimes, and path a2 the 2DD, 2DSD and 3DSD regimes. Two vertical paths (series b1 and b2) allow a systematic study of $\bar{B}$ as function of $\bar{d}$ through the 3DD and 2DD polymer confinement regimes for the b1 series and through the 3DSD and 2DSD regimes for the b2 series. Note that for the (b) series, both electrostatic and polymer-mediated interactions vary along the path, whereas along the (a) paths, only the polymer-mediated interaction should vary.

In all samples, the alcohol to surfactant weight ratio stays fixed $m_{\rm hex}/m_{\rm CPCl} = 0.9$. Two polymer molecular weights ($M_{\rm n} = 360\,000$ g/mole and $M_{\rm n} = 10\,000$ g/mole) were used in order to attein the two dilute confinement regimes.

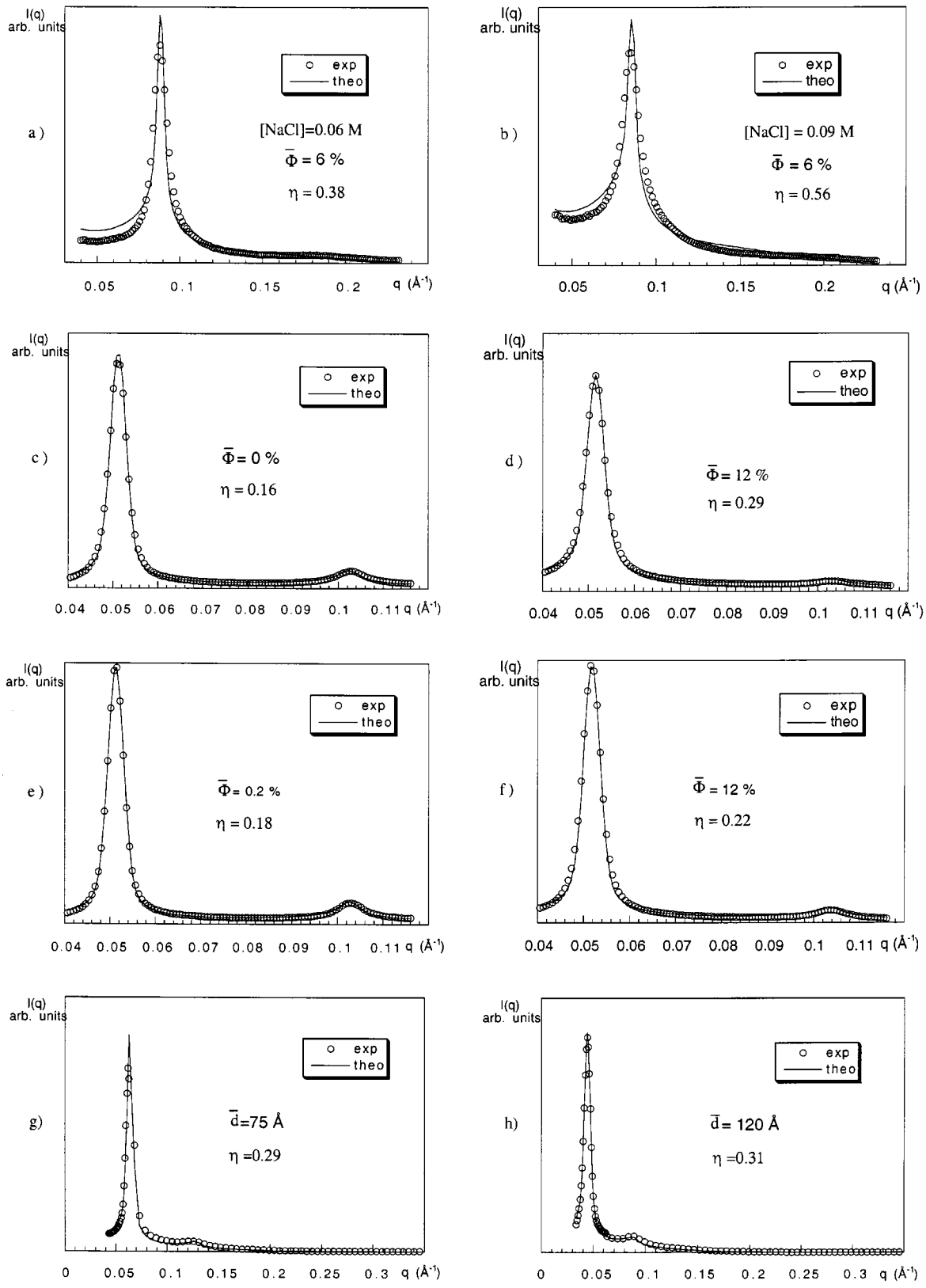

Fig. 4. Example of selected samples of the X-ray (a-f) and neutron (g, h) scattering intensity profiles fitted using equation (2). Open circles: experimental data; plain lines: best fits; (a, b): $\bar{\Phi} = 6\%$ and $\bar{d} = 50$ Å, (c-f): $\bar{d} = 100$ Å, (g): $\bar{\Phi} = 1\%$, (h): $\bar{\Phi} = 5\%$.

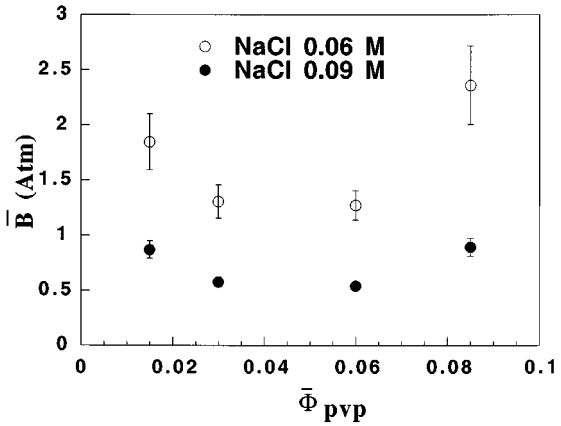

Fig. 5. Smectic compression modulus $\bar{B}$ (Atm) *vs.* polymer volume fraction in the solvent $\bar{\Phi}$ for $\bar{d} = 50$ Å, at two different salinities. The difference between the first sample series (open circles) of salinity [NaCl] = 0.06 mol/l and the second samples series (solid circles) of salinity [NaCl] = 0.09 mol/l) is almost constant $\Delta\bar{B} \approx 0.7$ Atm.

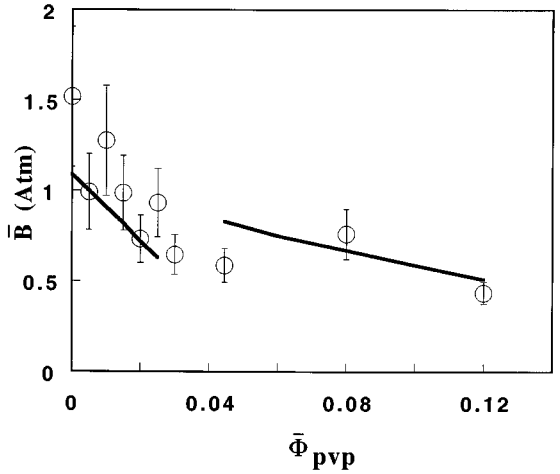

Fig. 6. Smectic compression modulus (Atm) *vs.* polymer volume fraction in the solvent (in this series PVP has a number average molecular weight $M_n = 10{,}000$) with a constant smectic periodicity $d = 126$ Å. The crossover between the 3DD and 3DSD regimes is close to $\bar{\Phi} \approx 2{-}4\%$. The experimental values of $\bar{B}$ were obtained using the measured parameter η and from equation (5). The plain curves are the theoreticaly predicted values of the layer compression modulus.

4.1 Variation of $\bar{B}$ as function of $\bar{\Phi}$ (series a1 and a2)

4.1.1 3DD and 3DSD polymer confinement regimes (series a1 and a2)

We used PVP with an average molecular weight $M_n = 10\,000$ g/mole. The boundary between 3DD and 2DD dilute regimes is then $\bar{d}/a \approx 15$ Å, and the overlap threshold is roughly $\bar{\Phi}^* \approx N^{-4/5} \approx 3\%$. The membrane volume fraction of the L_α phase was kept constant ($\psi = 21\%$, this corresponds to $\bar{d} = 100$ Å) for all the samples. The volume fraction of polymer in the solvent has been varied from 0 to 12%. Samples with a polymer concentration $\bar{\Phi} < 3\%$ (respectively $> 3\%$) correspond to a 3DD (3DS-D respectively) polymer-confinement regime.

Figures 4c-4d show the X-ray intensity profiles and the corresponding best fits for two samples of this series. In Figure 6 we have plotted the measured values of $\bar{B}$ *versus* $\bar{\Phi}$ as well as the theoretically predicted values for $\bar{B}$, which are obtained as the sum of each contribution (Eq. (10)). $\bar{B}_\mu^{\rm pol}$ is calculated from equations (7a), or (7b), regarding the confinement regime, $\bar{B}^{\rm elec}$ is calculated from equation (8a), and $\bar{B}^{\rm und}$ from equation (9). The theoretical expressions for $\bar{B}_\mu^{\rm pol}$ are valid only far from the crossovers between the various polymer confinement regimes. This is why, we did not compute $\bar{B}_\mu^{\rm pol}$ in the vicinity of $\bar{\Phi}^* \approx 3\%$. There is a good agreement between theory and experiments. In particular we observe that $\bar{B}$ decreases with $\bar{\Phi}$ faster in the 3DD regime than in the 3DSD regime as expected theoretically ($\bar{B}_\mu^{\rm pol} \propto -\bar{\Phi}$ in the 3DD regime and $\bar{B}_\mu^{\rm pol} \propto -\bar{\Phi}^{3/4}$ in the 3DSD regime).

4.1.2 2DD, 2DSD and 3DSD polymer confinement regimes (series a2)

We used PVP with an averaged molecular weight $M_n = 360\,000$ g/mol setting the boundary between 3DD and 2DD regimes to $\bar{d}/a \approx 120$ Å. We kept the same membrane volume fraction for the L_α phase: $\psi = 21\%$ ($\bar{d} = 100$ Å). The volume fraction of the polymer in the solvent has been varied between 0 and 12%. The 2DD regime is defined over the range $\bar{\Phi} < 0.3{-}0.7\%$; the 2DSD regime lies within the interval $0.3 - 0.7\% < \bar{\Phi} < 1{-}3\%$, and the 3DSD regime ranges at $\bar{\Phi} > 1{-}3\%$.

Figures 4e and 4f show X-ray intensity profiles and the corresponding best fits for two samples of this series. In the 2DD dilute regime, the polymer contribution to the layer compression modulus decreases with the polymer concentration ($\bar{B}_\mu^{\rm pol} \propto -\bar{\Phi}$), in contrast with the 2DSD regime, for which the polymer contribution increases with the polymer concentration ($\bar{B}_\mu^{\rm pol} \propto -\bar{\Phi}^{-1}$). In the 3DSD regime, the polymer contribution decreases also with the polymer concentration ($\bar{B}_\mu^{\rm pol} \propto -\bar{\Phi}^{3/4}$). Therefore, the smectic compression modulus is expected to be a non-monotonic function of the polymer concentration in this series. The experimental results plotted together with the theoretical values of $\bar{B}$ (Eqs. (7b-d, 8a)) in Figure 7 substantiate these predictions, despite the fact that the predicted values seem to be slightly under evaluated. One possible explanation is the uncertainty of the numerical prefactors in the theoretical expression for $\bar{B}_\mu^{\rm pol}$ in three regimes of confinement (3DD, 2DD and 2DSD), and the woolliness of the experimental boundaries between the various confinement regimes due to the strong polydispersity of the polymer.

4.2 Variation of $\bar{B}$ as function of $\bar{d}$ (series b1 and b2)

In these two series of experiments we fix the polymer volume fraction in the solvent and vary the lamellar

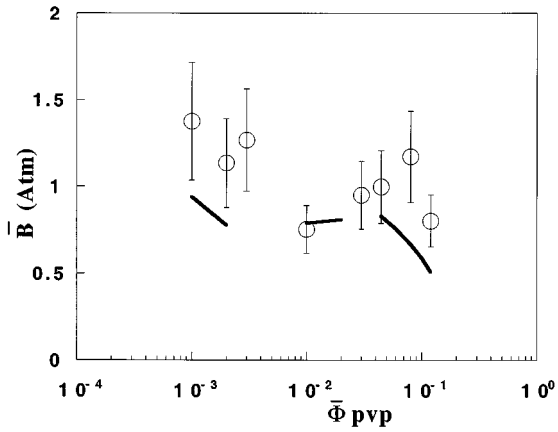

Fig. 7. Plot of the smectic compression modulus (Atm) as a function of the polymer volume fraction in the solvent (in this series PVP has a number average molecular weight M_n = 360,000) in the 2DD, 2DSD and 3DSD polymer confinement regimes. The crossover between the 2DD and 2DSD regimes is close to $\bar{\Phi} \approx 0.3-0.7\%$. The crossover between the 2DSD and 3DSD regimes is close to $\bar{\Phi} \approx 1-3\%$. The constant smectic periodicity is $d = 100$ Å. The plain lines are the theoretical predicted values.

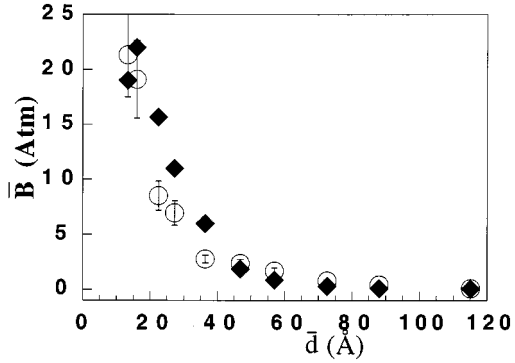

Fig. 8. Experimental (circles) smectic compression modulus (Atm) *versus* $\bar{d}$ (M_n = 10,000). Constant polymer volume fraction in the solvent: $\bar{\Phi} = 1\%$ [NaCl] = 0.03 mol/l. The crossover between the 3DD and 2DD regimes is close to $\bar{d} \approx 45$ Å. The experimental values of $\bar{B}$ were obtained using fitted η parameter and expression (1). Theoretical values: (diamonds).

spacing, which corresponds to vertical displacements in the polymer-confinement diagram. We used PVP with an averaged molecular weight $M_n = 10\,000$ g/mole. Note that for this series of experiments, both polymer-mediated and electrostatic interactions vary along the dilution paths, leading to a more difficult analysis of the results.

4.2.1 3DD and 2DD polymer confinement regimes (series b1)

The volume fraction of the polymer in the solvent is lower than the overlap threshold $\bar{\Phi}^*$ and is kept constant for all the samples ($\bar{\Phi} = 1\%$). The average thickness $\bar{d}$ of the solvent layer between two neighboring membranes has been varied from 18 to 120 Å. The crossover between the 3DD 2DD regimes is around $\bar{d} \approx 45$ Å. We were constrained to use brine of low salinity ([NaCl] = 0.03 mol/l) rather than pure water as solvent, in order to be able to measure significant variations in the Caillé parameter η. However, doing so, fits of the scattering patterns are less good, particularly for the more concentrated lamellar phases. Figure 4g shows the neutron scattering profile and the corresponding best fit of a selected sample of this series. Figure 8 shows the measured variations of the layer compression modulus (circles) and the calculated values (diamonds) as a function of $\bar{d}$. The theoretical values have been calculated by adding the contributions of each interaction to $\bar{B}$ using equation (8b) for the electrostatic part, equations (7a, 7c) for the polymer contribution depending on the confinement regimes, and equation (9) for the Helfrich's interaction. The most interesting feature is the rough exponential decrease of $\bar{B}$ as function of $\bar{d}$, reflecting the behavior of the electrostatic contribution. However, the polymer contribution can not be omitted, because neglecting this negative contribution would lead to a much to high value for $\bar{B}$. As an example, consider the sample with $\bar{d} = 16$ Å one measures $\bar{B}^{\rm exp} \simeq 19$ Atm whereas the theoretical contributions are expected to be $\bar{B}^{\rm elec} \simeq 27$ Atm, $\bar{B}^{\rm pol}_{\rm 2DD} \simeq -26$ Atm, and $\bar{B}^{\rm und} \simeq 21$ Atm. Note that the Helfrich's interactions are not negligible in the 2DD regime. In summary, these results show a good qualitative agreement between theory and experiment, however, we cannot expect quantitative predictions for the polymer contributions to $\bar{B}$, in the 2DD and 3DD regimes, for the same reasons as explained above.

4.2.2 3DSD and 2DSD regimes (series b2)

In this last series, the volume fraction of polymer in the solvent was kept constant $\bar{\Phi} = 5\%$, greater than the estimated overlap threshold $\bar{\Phi}^*$. The average thickness of the solvent has been varied in the range 18−120 Å. The boundary between the 2DSD and 2DD regimes is close to $\bar{d} \approx 1.5$ Å ($\bar{d}/a = 1/N\bar{\Phi}^2$) and the boundary between the 3DSD and 2DSD regimes is close to $\bar{d} = 30$ Å. We fixed the salinity: [NaCl] = 0.01 mol/l for the same reason as above.

Figure 4h shows the neutron-scattering profile and the corresponding best fit of a selected sample of this series. In Figure 9, we have plotted the experimental layer compression modulus *versus* the solvent layer thickness $\bar{d}$. For the four more dilute samples, the variation of $\bar{B}$ is controlled by the electrostatic contribution. Indeed the polymer contribution (3DSD polymer confinement regime) – as well as the Helfrich's one – are small in comparison with the electrostatic contribution. Therefore, $\bar{B}$ exhibits an exponential decrease with respect to $\bar{d}$ as expected. For the more concentrated samples (2DSD and 2DD regimes) we have failed to account the variations of $\bar{B}$ as function of $\bar{d}$, which seems quite complex. Such a behavior is certainly governed by the crossing from the 3SDD to the 2SDD

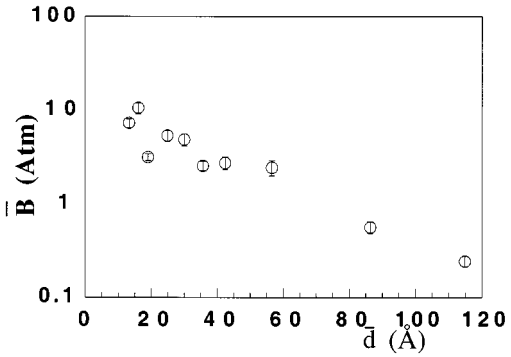

Fig. 9. Experimental smectic compression modulus (Atm) as a function of $\bar{d}$. ($M_n = 10{,}000$). Constant volume polymer volume fraction in the solvent: $\bar{\Phi} \approx 5\%$. [NaCl] = 0.01 mol/l. The crossover between 2DSD and 3DSD is close to $\bar{d} \approx 56$ Å.

and finally 2DD regimes of polymer confinement. However, a quantitative comparison between the model and the experiments is impossible for the following reasons: on one hand, on needs to keep in mind that the analytical expressions of the polymer contributions to $\bar{B}$ are valid only far away from the crossovers between the different regimes of polymer confinement. Unfortunately such restrictive conditions cannot be experimentally checked in our system (concerning the $\bar{d}$ variations). On the other hand the strong polydispersity of the polymer, leads to a blurred definition of these crossovers, and consequently to even more puzzling interpretation.

5 Conclusion

The successful fitting of the broad spectra of powder samples of polymer-containing surfactant lamellar phases confirms the great efficiency of the model suggested by Nallet *et al.* model, for the experimental study of intermembrane interactions in *stiff* lyotropic smectics. We have performed systematic measurements of the smectic compression modulus $\bar{B}$ of a lamellar phase containing a non adsorbing water soluble polymer. These measurements have been compared with a recent model of ours which predict the contribution of the polymer-mediated intermembranar interaction to $\bar{B}$ in the four expected regimes of polymer confinement. Several aspects of this work have been successful:

- We have shown unambiguously that the polymer-mediated interactions are destabilizing as expected theoretically.
- We have shown experimentally the additivity of the polymer-mediated and electrostatic interactions.
- We have obtained a quantitative agreement between theory and experiment in one of the regimes of polymer confinement *i.e.*, the 3DSD regime for which the polymer-mediated interaction arises essentially from the polymer depletion in the vicinity of the bilayers.
- A qualitative agreement has been checked between the model and the measurements of the variations of $\bar{B}$ as a function of the polymer concentration. In particularly, the non-monotonic behavior of $\bar{B}$ with respect to the polymer concentration through out the various regimes of polymer confinement has been evidenced.

This experimental study has also displayed some weaknesses of our theoretical model: the limited range of validity of the theoretical expressions in the 2DD and 2DSD regimes, as well as the uncertainty concerning some numerical prefactors in these expressions (inherent in our analytical approach) did not allow to a draw clear conclusion for the dependence of $\bar{B}$ on the intermembrane distance $\bar{d}$. Despite these limits, this work realizes a first attempt (to our knowledge) of a systematic experimental study of the thermodynamics of polymer confinement within infinite slits.

The authors are indebted to G. Porte for countless helpful discussions, They are grateful to O. Diat for his help and hospitality at ESRF on the X-ray scattering. They also aknowledge discussions with D. Roux. Finally, they would thank E. Eiser for a careful reading of the manuscript.

References

1. D. Roux, C.R. Safinya, J. Phys. France **49**, 307 (1988).
2. W.Z. Helfrich, Naturforsch. A **33**, 305 (1978).
3. P. Kékicheff, B. Cabane, M. Rawiso, J. Colloid Interface Sci. **102**, 51 (1984).
4. C. Ligoure, G. Bouglet, G. Porte, Phys. Rev. Lett. **71**, 3600 (1993).
5. C. Ligoure, G. Bouglet, G. Porte, O. Diat, J. Phys. II France **7**, 473 (1997).
6. G. Bouglet, C. Ligoure, A.M. Bellocq, E. Dufourc, G. Mosser, Phys. Rev. E. **57**, 834 (1998).
7. L. Porcar, C. Ligoure, J. Marignan, J. Phys. II France **7**, 493 (1997).
8. M. Shing, R. Ober, M. Kleman, J. Phys. Chem. **97**, 11108 (1993).
9. M.F. Ficheux, A.M. Bellocq, F. Nallet, J. Phys. II France **5**, 823 (1995).
10. E.Z. Radlinska, T. Gulik-Krzywicki, F. Lafuma, D. Langevin, W. Urbach, C.E. Williams, R. Ober, Phys. Rev. Lett. **74**, 4237 (1995); E.Z. Radlinska, T. Gulik-Krzywicki, F. Lafuma, D. Langevin, W. Urbach, C.E. Williams, J. Phys. II France **7**, 1393 (1997).
11. I. Illioupoulos, U. Olsson, J. Phys. Chem. **98**, 1500 (1994).
12. B. Demé, M. Dubois, T. Zemb, B. Cabanne, J. Phys. Chem. **100**, 3828 (1996).
13. H.E. Warriner, S.H. Idziak, N.L. Slack, P. Davidson, C.R. Safinya, Science **271**, 969 (1996).
14. S.H. Warriner, P. Davidson, N. Slack, M. Schellhorn, P. Eiselt, S.H.J. Idziak, H.-W. Schmidt, C. Safinya, J. Chem. Phys. **107**, 9 (1997).
15. F. Nallet, D. Roux, C. Quilliet, P. Fabre, S.T. Milner, J. Phys. II France **4**, 1477 (1994).
16. G. Porte, J. Marignan, P. Bassereau, R. May, J. Phys. France **38**, 511 (1984).
17. M. Daoud, P.-G. de Gennes, J. Phys. France **38**, 85 (1977).
18. J.T. Brooks, M.E. Cates, J. Chem. Phys. **99**, 5464 (1993).

19. Neutron scattering experiments have been previously performed in order to sudy the structure of confined polymer chains in cylindrical pores: J. Lal, S.K. Sinha, L. Auvray, J. Phys. II France **7**, 1597 (1997).
20. A. Caillé, C. R. Acad. Sci. Paris B **274**, 1733 (1972).
21. L. Gunther, Y. Imry, J. Lajzerowicz, Phys. Rev. A **22**, 1733 (1980).
22. G. Porte, J. Marignan, P. Bassereau, R. May, Europhys. Lett. **7**, 713 (1988).
23. F. Nallet, R. Laversanne, D. Roux, J. Phys. II France **3**, 487 (1993).
24. R. Zhang, R.M. Suter, J.F. Nagle, Phys. Rev. E **50**, 5047 (1994).
25. N. Lei, C.R. Safinya, R.F. Bruinsma, J. Phys. II France **5**, 425 (1995).
26. R. Zhang, S. Tristam-Nagle, W. Sun, R.L. Headrick, T.C. Irving, R.M Suter, J.F. Nagle, Biophys. J. **70**, 349 (1996).
27. J. Lemmich, K. Mortensen, J.H. Ipsen, T. Honger, R. Bauer, O.G. Mouritsen, Phys. Rev. E. **53**, 5169 (1996).
28. J.T. Brooks, Ph.D. thesis, University of Cambridge, 1993.
29. R. Oda, J.D. Lister, J. Phys. II France **7**, 815 (1997).
30. M. Kurata, M. Stockmaker, Fortschr. Hochpolym. Forsch **3**, 196 (1963).
31. R. Meza, L. Gargallo, Europ. Polym. J. **13**, 235 (1977).
32. P. Bösecke, O. Diat, B. Rasmussen, Rev. Sci. Instrum. **66**, 1636 (1995).
33. F. Castro-Roman, G. Porte, C. Ligoure, Phys. Rev. Lett. **82**, 109 (1999).
34. Since the polymer volume fraction profile between to bilayers is not known, it is replaced by an effective uniform polymer volume fraction (which should be close to the average polymer volume fraction in the solvent $\bar{\Phi}$). For neutron experiments, we have checked that the fitted scaling vector A_0 is close to the expected one with $\rho_{\rm s} = \left(1 - \bar{\Phi}\right) \rho_{\rm D_2O} + \bar{\Phi} \rho_{\rm PVP}$.
35. M. Dubois, T. Zemb, L. Belloni, A. Delville, P. Levitz, R. Setton, J. Chem. Phys. **96**, 2278 (1992).
36. B.Y. Zaslavsky, L.M. Mihevva, M.N. Rodnikova, G. Spivak, V.S. Harki, A.U. Mahmudov, Chem. Soc. Faraday Trans. I **85**, 2857 (1989).